

Reconstructing the 125GeV SM Higgs boson through $\ell\bar{\ell}\gamma$

Long-Bin Chen^{1*}, Cong-Feng Qiao^{1,2†}, and Rui-Lin Zhu^{1‡}

¹*Department of Physics, Graduate University of the Chinese Academy of Sciences,
YuQuan Road 19A, Beijing 100049, China*

²*Kavli Institute for Theoretical Physics China,
the Chinese Academy of Sciences, Beijing 100190, China*

Abstract

To ascertain the new boson with mass near 125 GeV observed recently by ATLAS and CMS Collaborations to be the Standard Model Higgs, and to determine its intrinsic properties, more measurements on its various decay channels are still necessary. In this work we reanalyze the processes of the Standard Model Higgs radiative decays to lepton pairs. We find that when photon and leptons are hard, that is possessing energies larger than 1 GeV, the branching fractions of $H \rightarrow \ell\bar{\ell}\gamma$ ($\ell = e$ or μ) processes are about two-thirds of the $H \rightarrow \mu^+\mu^-$ process. Since the lepton-pair yields of the radiative processes mainly come from the Z-boson conversion, which will greatly suppress the backgrounds, we believe the signal should be observable in presently accumulated data or in the next run of the LHC experiment, provided the Standard Model Higgs is indeed light.

PACS number(s): 12.15.Ji, 12.15.Lk, 14.80.Bn

* E-mail: chenglogbin10@mails.gucas.ac.cn

† E-mail: qiaocf@gucas.ac.cn

‡ E-mail: zhuruilin09@mails.gucas.ac.cn

I. INTRODUCTION

The recent discovery of a Standard Model(SM) Higgs-like boson with mass near 125GeV by ATLAS [1] and CMS [2] Collaborations in Large Hadron Collider(LHC) experiment stirs the world with a great interest in high energy physics. Following, to identify whether it is the SM Higgs boson or not, and to understand further its nature are of the utmost goals in high energy physics. In order to ascertain the new finding is just the SM Higgs boson, but not others, more measurements on its decays are necessary. Therefore, to hunt for more LHC experiment accessible Higgs processes is an important task for theoretical study.

In ATLAS and CMS experiments, the SM Higgs-like particle was observed via its five decay channels, i.e., to $\gamma\gamma$, $Z^{(*)}Z$, $W^{(*)}W$, $\tau^+\tau^-$ and $b\bar{b}$. All these decay processes are, at least intermediately, in two-body decay mode. In this paper, we propose to study a complementary channel, the three-body lepton-pair radiative decay processes $H \rightarrow \ell\bar{\ell}\gamma$ (ℓ stands for leptons), to reconstruct the SM Higgs-like neutral boson around 125GeV. Due to the enhancement induced by internal heavy quarks and gauge bosons, we find that these three-body decay processes will not be suppressed much relative to the pure lepton-pair decay modes, and are observable with the data collected in 2011 and 2012.

Before the LHC run, some of the radiative lepton-pair decay processes were analyzed [3–5], where [3] considered only the light fermions and hence neglected the tree diagram contribution; [4] evaluated the Higgs boson radiative decay to muon pair with Next-to-Leading Order(NLO) corrections; the calculation in [5] was incomplete; and in all these analyses the realistic LHC experimental conditions were not fully considered. In this work, we calculate completely the SM Higgs radiative decays to lepton pairs under the helicity basis, which may issue more information about the Higgs boson. Various physical cuts for reconstructing the Higgs boson in LHC experiment are applied in the calculation. The partial decay width with respect to the invariant mass of the muon pair is given in order to disentangle the SM Higgs with Higgs bosons in other models [6]. The $H \rightarrow \tau^+\tau^-\gamma$ process is also calculated beyond the Born level, where the tau mass

is non-negligible. Although in this process the leading order tree diagrams contribute dominantly, we find the NLO contribution is very helpful in experimental measurement due to the Z-pole effect, which may greatly suppress the background.

Recently, Gastmans, Wu and Wu pointed out that the dimensional regularization scheme may possess some shortcomings in the calculation of Higgs to diphoton decays [7, 8]. More explicitly, they believe that the W-loop contribution should decouple when taking the zero-mass limit for W boson. However, it is not the case in real calculation in dimensional regularization scheme [9]. Their works stimulated many discussions on this point in the literature [10–14]. Since in this work we also encounter the triangle-loop diagrams appearing in the Higgs to diphoton decays process, we will check again whether the W-boson decouples or not in the massless limit.

The remainder of the paper is arranged as follows. In Sec. II, the analytical formulae for the concerned processes are presented and the W-boson decouple assumption is also confronted. In Sec. III, we give out our numerical results and related phenomenological discussions. The last section is devoted to conclusions.

II. FORMULAE

A. The Born amplitude

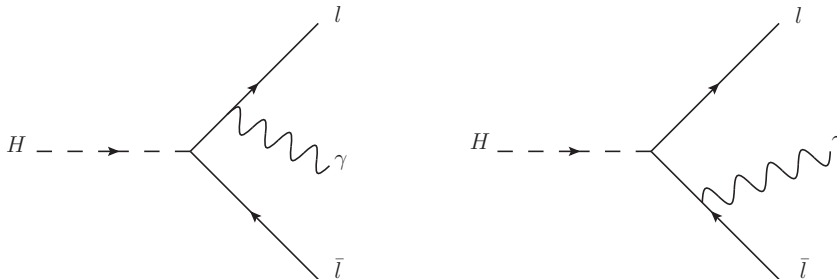


FIG. 1: The tree level diagrams of Higgs boson radiative decays to lepton pairs.

At tree level, there are only two Feynman Diagrams for the Higgs boson radiative decays to lepton pairs, which are shown in Fig. 1. For the convenience of following discussions, the momenta of particles are reassigned as: $p_1 = p_H$, $p_2 = p_\gamma$, $k_1 = p_\ell$, and $k_2 = p_{\bar{\ell}}$. The Mandelstam invariants are defined as $s = (k_1 + k_2)^2$, $t = (k_2 + p_2)^2$, $u = (k_1 + p_2)^2$, and $s + t + u = 2m_\ell^2 + m_H^2$. After doing some simplification, the tree level amplitude can be expressed as

$$\mathcal{M}_{tree} = \frac{e^2 m_l}{2m_W s_W} \left\{ \frac{\bar{u}(k_1) \not{p}_2 \not{\epsilon} v(k_2) - 2\varepsilon \cdot k_1 \bar{u}(k_1)(k_2)}{u - m_\ell^2} + \frac{\bar{u}(k_1) \not{p}_2 \not{\epsilon} v(k_2) + 2\varepsilon \cdot k_2 \bar{u}(k_1)v(k_2)}{t - m_\ell^2} \right\}. \quad (1)$$

B. The One-Loop Amplitudes

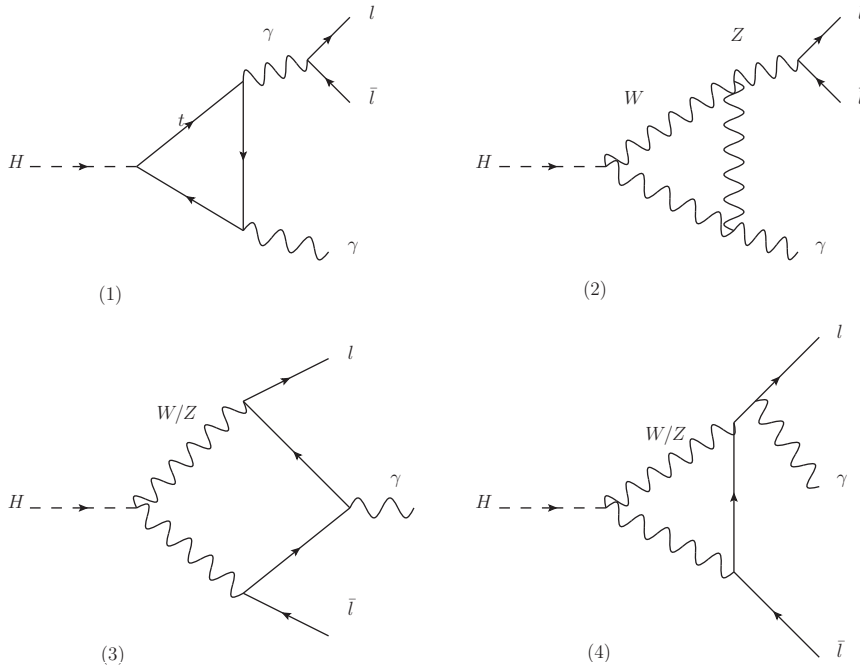


FIG. 2: The typical loop diagrams of Higgs boson radiative decays to lepton pairs.

For the concerned processes, the next-to-leading order contribution is very important for at least two reasons. First, the large couplings of Higgs boson with heavy fermions

and gauge bosons greatly enhance the decay rates at NLO. Secondly, the intermediate Z-boson decays may greatly reduce the backgrounds and enable the experimental measurement on signals more transparent.

The typical one-loop Feynman diagrams are shown in Fig. 2. In our calculation, both tree level and NLO amplitudes are generated by virtue of the Mathematica package FeynArts [15]. The analytical calculation of the amplitudes proceeds with the help of package FeynCalc [16]. Through out the calculation, the Feynman-'t Hooft gauge is adopted, and for the convenience of calculation and discussion, the one-loop Feynman diagrams are classified into four groups, i.e., 1) the group of triangle diagrams with virtual photon directly coupling to $\ell\bar{\ell}$; 2) the group of triangle diagrams with virtual Z-boson directly coupling to $\ell\bar{\ell}$; 3) the group of W- or Z-box diagrams, and 4) the group of triangle diagrams with a photon emitting from leptons.

In Feynman-'t Hooft gauge, there are 28 triangle diagrams in the first group. After doing some algebraic reduction and simplification the amplitude in this group can be expressed as

$$\mathcal{M}_\gamma = \mathcal{M}_\gamma^t + \mathcal{M}_\gamma^W, \quad (2)$$

where the amplitudes for top quark and W boson(including Goldstone and ghost) induced diagrams read

$$\begin{aligned} \mathcal{M}_\gamma^t = & \frac{-m_t^2 e^4 N_c}{18\pi^2 m_W \sin \theta_W s (m_H^2 - s)^2} \{ (m_H^2 - s) ((m_H^2 - s - 4m_t^2) \times \\ & C_0(m_H^2, 0, s, m_t^2, m_t^2, m_t^2) - 2) + 2s (B_0(s, m_t^2, m_t^2) - B_0(m_H^2, m_t^2, m_t^2)) \} \times \\ & ((m_H^2 - s) \bar{u}(k_1) \not{\epsilon} v(k_2) - 2\varepsilon \cdot p_1 \bar{u}(k_1) \not{\epsilon} v(k_2)), \end{aligned} \quad (3)$$

and

$$\begin{aligned}
\mathcal{M}_\gamma^W &= \frac{e^4}{16\pi^2 m_W \sin \theta_W s (m_H^2 - s)^2} \{ (m_H^2 - s)(m_W^2(m_H^2 - s)(6m_H^2 - 12m_W^2 - 5s) \times \\
&C_0(m_H^2, 0, s, m_t^2, m_t^2, m_t^2) - (m_H^2 + 6m_W^2)(sB_0(m_H^2, m_W^2, m_W^2) - sB_0(s, m_W^2, m_W^2) \\
&+ m_H^2 - s))\bar{u}(k_1) \not{z}v(k_2) - 2(-2m_W^2(m_H^2 - s)(-3m_W^2 + 6m_H + 4s) \times \\
&C_0(m_H^2, 0, s, m_t^2, m_t^2, m_t^2) - (m_H^2 + 6m_W^2)(sB_0(m_H^2, m_W^2, m_W^2) - sB_0(s, m_W^2, m_W^2) \\
&+ m_H^2 - s))\varepsilon \cdot p_1 \bar{u}(k_1) \not{p}_2 v(k_2) \} , \tag{4}
\end{aligned}$$

respectively. Since the bottom quark mass is about two orders smaller than the top quark mass, and the electric charge of bottom quark is half of top quark, it is reasonable to neglect the contribution of b-quark loop diagram. Note that the above amplitudes contain neither ultraviolet nor infrared divergences. The C_0 and B_0 functions are defined the same as in Ref. [17]. The value of the C_0 function and the finite part of the B_0 function can be readily obtained by LoopTools [17], and they have also been checked with analytical results.

To see whether the W-loop decouples from the decay amplitude or not, we take a cut on the virtual photon propagators in the group one diagrams, i.e., take the zero limit for Mandelstam variable s , and then factorize out the photon polarization vector. After doing these, the amplitude \mathcal{M}_γ^W turns to be

$$\begin{aligned}
\mathcal{M}_{s=0}^{cut} &= -\frac{ie^3}{16\pi^2 m_W \sin \theta_W m_H^2} ((k_1 + k_2)^\mu p_2^\nu - g^{\mu\nu} m_H^2) \{ 2m_H^2 + 12m_W^2 + 12m_W^2(2m_W^2 \\
&- m_H^2)C_0(m_H^2, 0, 0, m_W^2, m_W^2, m_W^2) \} , \tag{5}
\end{aligned}$$

which is in agreement with results obtained in Refs. [10, 11]. This confirms that the W-boson loop contribution will not decouple from the amplitude in the zero mass limit. Moreover, while taking the zero limit for s in top-loop amplitude, we get the same result as (4.11) of Ref. [11], which in some sense convinces us of our calculation.

Similar to \mathcal{M}_γ , there are also 28 triangle diagrams in group two with virtual Z boson directly coupling to the lepton pairs. Here, the ultraviolet divergence appears, which can

be renormalized by adding proper counter terms in the on-shell renormalization scheme as given in Ref. [18]. In the end, we get the finite amplitude as

$$\mathcal{M}_Z = \mathcal{M}_Z^t + \mathcal{M}_Z^W, \quad (6)$$

where the sub-amplitudes for top-quark and W-boson(including Goldstone and ghost) induced loop diagrams read

$$\begin{aligned} \mathcal{M}_Z^t = & \frac{m_t^2 e^4 N_c}{576\pi^2 \sin^3 \theta_W \cos^2 \theta_W m_W (m_H^2 - s)^2 (s - m_Z^2 + i\Gamma_Z m_Z)} (8 \sin^2 \theta_W - 3) \{ \\ & (m_H^2 - s) ((s - m_H^2 + 4m_t^2) C_0(m_H^2, 0, s, m_t^2, m_t^2, m_t^2) + 2) + 2s B_0(m_H^2, m_t^2, m_t^2) \\ & - 2s B_0(s, m_t^2, m_t^2) \} ((m_H^2 - s) (\bar{u}(k_1) \not{\epsilon} \gamma^5 v(k_2) + (4 \sin^2 \theta_W - 1) \bar{u}(k_1) \not{\epsilon} v(k_2)) \\ & - 2\varepsilon \cdot p_1 (\bar{u}(k_1) \not{p}_2 \gamma^5 v(k_2) + (4 \sin^2 \theta_W - 1) \bar{u}(k_1) \not{p}_2 v(k_2))) \\ & - \frac{im_t^2 e^4 N_c}{96\pi^2 \sin^3 \theta_W \cos^2 \theta_W m_W (m_H^2 - s) (s - m_Z^2 + i\Gamma_Z m_Z)} \{ \\ & (\epsilon^{\mu\nu\rho\sigma} p_{1\rho} p_{2\sigma} ((m_H^2 - s) C_0(m_H^2, 0, s, m_t^2, m_t^2, m_t^2) + 2B_0(m_H^2, m_t^2, m_t^2) \\ & - 2B_0(s, m_t^2, m_t^2))) \} \varepsilon_\mu (\bar{u}(k_1) \gamma_\nu \gamma^5 v(k_2) + (4 \sin^2 \theta_W - 1) \bar{u}(k_1) \gamma_\nu v(k_2)), \quad (7) \end{aligned}$$

$$\begin{aligned}
\mathcal{M}_Z^W &= \frac{e^4}{128\pi^2 m_W \sin^3 \theta_W \cos^2 \theta_W (m_H^2 - s)(s - m_Z^2 + i\Gamma_z m_Z)} \{ \\
&2(m_H^2 - s)((3s - 5m_H^2 + 13m_W^2) \cos^2 \theta_W + (m_H^2 - 2s + m_W^2) \sin^2 \theta_W) \times \\
&m_W^2 C_0(m_H^2, 0, s, m_W^2, m_W^2, m_W^2) + (\cos^2 \theta_W (m_H^2 + 10m_W^2) \\
&-(m_H^2 + 2m_W^2) \sin^2 \theta_W)(m_H^2 - s + sB_0(m_H^2, m_W^2, m_W^2) \\
&-sB_0(s, m_W^2, m_W^2)) \} (\bar{u}(k_1) \not{\epsilon} \gamma^5 v(k_2) + (4 \sin^2 \theta_W - 1) \bar{u}(k_1) \not{\epsilon} v(k_2)) \\
&+ \frac{e^4}{64\pi^2 m_W \sin^3 \theta_W \cos^2 \theta_W (m_H^2 - s)^2 (s - m_Z^2 + i\Gamma_z m_Z)} \{ \\
&-2(m_H^2 - s)((6s - 5m_H^2 + 10m_W^2) \cos^2 \theta_W + (m_H^2 - 2s - 2m_W^2) \sin^2 \theta_W) \times \\
&m_W^2 C_0(m_H^2, 0, s, m_W^2, m_W^2, m_W^2) - (\cos^2 \theta_W (m_H^2 + 10m_W^2) \\
&-(m_H^2 + 2m_W^2) \sin^2 \theta_W)(m_H^2 - s + sB_0(m_H^2, m_W^2, m_W^2) \\
&-sB_0(s, m_W^2, m_W^2)) \} \varepsilon \cdot p_1 (\bar{u}(k_1) \not{\epsilon} \gamma^5 v(k_2) + (4 \sin^2 \theta_W - 1) \bar{u}(k_1) \not{\epsilon} v(k_2)) \\
&+ \frac{m_\ell m_W e^4}{64\pi^2 \sin^3 \theta_W \cos^2 \theta_W (m_H^2 - s)(s - m_Z^2 + i\Gamma_z m_Z)} \{ \\
&2(m_H^2 - s)(2 \cos^2 \theta_W - \sin^2 \theta_W) C_0(m_H^2, 0, s, m_W^2, m_W^2, m_W^2) \\
&+ B_0(s, m_W^2, m_W^2) - B_0(m_H^2, m_W^2, m_W^2) \} \varepsilon \cdot p_1 \bar{u}(k_1) \gamma^5 v(k_2) , \tag{8}
\end{aligned}$$

respectively. In the limit of Z being on mass shell, we obtain the known decay amplitude for $H \rightarrow Z\gamma$, and our analytic result agrees with Ref. [3].

The calculation procedure for box diagrams is similar to what for the triangle diagrams, except it becomes more tedious and complicate. However, the analytic result for box diagrams is too lengthy to be presented in the paper.

Note that since the direct coupling of Higgs or Goldstone bosons to leptons are suppressed by factor of $\frac{m_\ell}{m_H}$, which is much less than one for light leptons, contributions of the corresponding diagrams to the final result are negligibly small. However, for τ lepton, those terms are kept due to its relatively large mass.

C. Helicity amplitudes

Notice that the helicity information on final states may tell more on parent particles, we also perform the calculation on the helicity basis for final states. Employing the helicity method given in Refs. [19, 20], by introducing a light-like momentum q_0 and a space-like vector q_1 with constraints $q_0 \cdot q_1 = 0$ and $q_1 \cdot q_1 = -1$, the helicity amplitudes can be then constructed as

$$\begin{aligned}
\mathcal{M}_{ss'\lambda} &= N_0 \text{Tr}[(\not{k}_2 - m_\ell)(1 - \gamma^5) \not{q}_0(\not{k}_1 + m_\ell)\mathcal{A}_\lambda] , \\
\mathcal{M}_{-s-s'\lambda} &= N_0 \text{Tr}[(\not{k}_2 - m_\ell)(1 + \gamma^5) \not{q}_0(\not{k}_1 + m_\ell)\mathcal{A}_\lambda] , \\
\mathcal{M}_{-ss'\lambda} &= N_0 \text{Tr}[(\not{k}_2 - m_\ell)(1 - \gamma^5) \not{q}_0 \not{q}_1(\not{k}_1 + m_\ell)\mathcal{A}_\lambda] , \\
\mathcal{M}_{s-s'\lambda} &= N_0 \text{Tr}[(\not{k}_2 - m_\ell) \not{q}_1(1 - \gamma^5) \not{q}_0(\not{k}_1 + m_\ell)\mathcal{A}_\lambda] .
\end{aligned} \tag{9}$$

Here, $N_0 = 1/\sqrt{16(q_0 \cdot k_1)(q_0 \cdot k_2)}$; $\mathcal{A}_\lambda = \mathcal{A}_\lambda^{tree} + \mathcal{A}_\lambda^{loop}$, which can be readily obtained after removing the spinors out from the above mentioned amplitude; $s = 1/2$ and $s' = 1/2$ denote for the spin projections of ℓ and $\bar{\ell}$ respectively; $\lambda = \pm 1$ represents the polarizations of the photon. Hence, in the end there will be eight different kinds of helicity amplitudes.

In the helicity method, the total unpolarized matrix element squared is just the sum of individual polarized matrix element squared, i.e.,

$$|\mathcal{M}|^2 = |\mathcal{M}_{ss'\lambda}|^2 + |\mathcal{M}_{-s-s'\lambda}|^2 + |\mathcal{M}_{-ss'\lambda}|^2 + |\mathcal{M}_{s-s'\lambda}|^2 . \tag{10}$$

In practice of our calculation, we find that the helicity method gives the same result of the total unpolarized matrix element squared as the traditional one, but the former provides more information about the physical process and in some case brings convenience in the calculation.

III. THE NUMERICAL CALCULATION

A. Input parameters and physical conditions

In numerical evaluation, the relevant inputs are taken as [21, 22]

$$\begin{aligned} m_t &= 172.0 \text{ GeV}, \quad m_W = 80.39 \text{ GeV}, \quad \alpha(m_Z) = 1/128, \quad \Gamma_Z = 2.48 \text{ GeV}, \\ m_Z &= 91.18 \text{ GeV}, \quad m_\mu = 0.105 \text{ GeV}, \quad m_e = 0.51 \text{ MeV}, \quad m_\tau = 1.776 \text{ GeV}. \end{aligned} \quad (11)$$

The SM Higgs mass is taken to be 125.5 GeV in our numerical evaluation, which is around the mass of the Higgs-like boson recently observed by ATLAS and CMS Collaborations [1, 2].

Formally, the three-body partial decay width can be expressed as

$$d\Gamma = \frac{1}{(2\pi)^3} \frac{1}{32m_H^3} |\mathcal{M}|^2 ds dt. \quad (12)$$

Before imposing any physical cuts, the Mandelstam variables s and t , defined previously, vary in space of

$$s_{max} = m_H^2, \quad s_{min} = 4m_\ell^2, \quad (13)$$

and

$$t_{max} = \frac{m_H^4}{4s} - \left(\sqrt{\frac{s}{4} - m_\ell^2} - \frac{m_H^2 - s}{2\sqrt{s}} \right)^2, \quad t_{min} = \frac{m_H^4}{4s} - \left(\sqrt{\frac{s}{4} - m_\ell^2} + \frac{m_H^2 - s}{2\sqrt{s}} \right)^2, \quad (14)$$

respectively.

Considering of the experimental constraints, certain physical cuts should be imposed on the phase space. In our calculation three sets of physical cuts are taken for s , t , u and momenta of final states, as presented in Table I. That is $s \geq (m_{\ell\bar{\ell}}^2)_{cut}$, $t \geq (m_{\ell\gamma}^2)_{cut}$, $u \geq (m_{\ell\gamma}^2)_{cut}$, $E_\ell \geq (E_\ell)_{cut}$, $E_{\bar{\ell}} \geq (E_{\bar{\ell}})_{cut}$, and $E_\gamma \geq (E_\gamma)_{cut}$, where the last three constraints are imposed in the center of mass system of Higgs boson. These cuts, especially the cut III, facilitates the experiment measurement on photon and leptons. Note that for Higgs radiative decay to τ pair, the low limits of lepton energies in cut I are taken to be

the τ mass, but rather the values given in Table I. In addition of the cuts in the table, in practice the experimental conditions are also taken into account [23]. That is, for CMS experiment the transverse momenta of photon and leptons should be larger than 15 GeV and 10 GeV(or 20 GeV) respectively, and the pseudo rapidity in experiment measurement is constrained within the fiducial volume of $|\eta| < 2.5$.

TABLE I: Selection cuts in numerical evaluation.

	$(m_{\ell\bar{\ell}}^2)_{\text{cut}}$	$(m_{\ell\gamma}^2)_{\text{cut}}$	$(m_{\bar{\ell}\gamma}^2)_{\text{cut}}$	$(E_{\ell})_{\text{cut}}$ (GeV)	$(E_{\bar{\ell}})_{\text{cut}}$ (GeV)	$(E_{\gamma})_{\text{cut}}$ (GeV)
cut I	$25m_{\mu}^2$	$25m_{\mu}^2$	$25m_{\mu}^2$	1	1	1
cut II	$50m_{\mu}^2$	$50m_{\mu}^2$	$50m_{\mu}^2$	6	6	6
cut III	$75m_{\mu}^2$	$75m_{\mu}^2$	$75m_{\mu}^2$	10	10	10

B. Numerical results and discussions

With the analytic expressions obtained, the input parameters given and the physical conditions selected in preceding sections, the decay widths and branching fractions of a 125.5 GeV SM Higgs boson radiative decays to lepton pairs can be readily obtained, which are shown in Table II and Table III. For these processes, the backgrounds are huge, of which the dominant ones come from the Drell-Yan + ISR(initial state radiation) and Drell-Yan + FSR(final state radiation) processes [23, 24]. The backgrounds are evaluated with the help of the package CalcHep [25], and the results are presented in Table IV. For illustration, the invariant mass distributions of the decay mode $H \rightarrow \mu^+\mu^-\gamma$ are shown in Figs. 3 and 4, for summed and individual helicity cases, respectively. For Higgs to $e^+e^-\gamma$ decay mode, result shows that contributions of tree and tree-loop interference terms are negligible, as mentioned in Ref. [4]. Hence, the invariant mass distribution of $H \rightarrow e^+e^-\gamma$ process tends to be as the NLO mass distribution of $H \rightarrow \mu^+\mu^-\gamma$ decay mode, that is the subtraction of the total contribution by the tree level contribution as shown in Fig. 3. For $H \rightarrow \tau^+\tau^-\gamma$ process, the dominant contribution comes from

the leading order diagrams, due to the relatively large Higgs- τ coupling. However, the subleading contribution for $H \rightarrow \tau^+\tau^-\gamma$ process from the internal Z conversion to τ pair tends to be meaningful with the help of Z-pole veto in experimental measurement.

TABLE II: The decay widths and branching fractions with various Cuts. Here, the mass of Higgs boson is taken to be 125.5GeV.

	$\Gamma_{e^+e^-\gamma}(10^{-7}\text{GeV})/Br(10^{-4})$	$\Gamma_{\mu^+\mu^-\gamma}(10^{-7}\text{GeV})/Br(10^{-4})$	$\Gamma_{\tau^+\tau^-\gamma}(10^{-6}\text{GeV})/Br(10^{-3})$
cut I	4.29/1.04	5.67/1.38	33.4/8.10
cut II	3.89/0.94	4.57/1.11	16.1/3.90
cut III	3.61/0.88	4.09/0.99	11.5/2.79

TABLE III: The decay widths and branching fractions with different transverse momentum cuts for leptons. The minimum transverse momentum for photon is set to be 15 GeV, the pseudo rapidity $|\eta|$ is constrained within 2.5, and the invariant mass cuts are taken to be the Cut III of Table I.

	$\Gamma_{e^+e^-\gamma}(10^{-7}\text{GeV})/Br(10^{-4})$	$\Gamma_{\mu^+\mu^-\gamma}(10^{-7}\text{GeV})/Br(10^{-4})$
$p_{\perp,\text{cut}}^\ell = 10\text{GeV}$	2.73/0.66	2.94/0.71
$p_{\perp,\text{cut}}^\ell = 20\text{GeV}$	2.11/0.51	2.28/0.55

Numerical evaluation indicates that the contributions of Box and triangle diagrams, in which the photon emits from one of the fermions, are tiny in comparison with what from the first two groups. Furthermore, among the loop diagrams those with a W triangle are primary for the decay processes. Since the triangle diagrams in our calculation have similar property to what of the Higgs to two photon process, we also check the W decoupling assumption by taking the zero mass limit, and find that W-loop contribution will not decouple in the dimensional regularization scheme.

Results show that the sum of the branching ratios of $H \rightarrow \mu^+\mu^-\gamma$ and $H \rightarrow e^+e^-\gamma$ processes with cut I is about two times bigger than that of $H \rightarrow \ell\bar{\ell}\ell\bar{\ell}(\ell = \mu \text{ or } e)$

TABLE IV: The background of Drell-Yan plus ISR or FSR photon. The cuts are of the same as in signal production in Table III. The invariant mass of $\ell\bar{\ell}\gamma$ lies in the scope of 115 – 180 GeV as in Ref. [23].

	ISR $p_{\perp,\text{cut}}^{\ell} = 10\text{GeV}$	ISR $p_{\perp,\text{cut}}^{\ell} = 20\text{GeV}$	FSR $p_{\perp,\text{cut}}^{\ell} = 10\text{GeV}$	FSR $p_{\perp,\text{cut}}^{\ell} = 20\text{GeV}$
$\sigma(e^+e^-\gamma)$	$3.24 \times 10^{-1}\text{pb}$	$2.78 \times 10^{-1}\text{pb}$	$1.27 \times 10^{-1}\text{pb}$	$1.02 \times 10^{-1}\text{pb}$
$\sigma(\mu^+\mu^-\gamma)$	$3.26 \times 10^{-1}\text{pb}$	$2.8 \times 10^{-1}\text{pb}$	$1.28 \times 10^{-1}\text{pb}$	$1.02 \times 10^{-1}\text{pb}$

processes [22], where no cut is employed, and also larger than the branching ratio of $H \rightarrow \mu^+\mu^-$ decay channel. Since $H \rightarrow \ell\bar{\ell}\ell\bar{\ell}$ ($\ell = \mu$ or e) processes have already been observed in LHC experiment, the Higgs radiative decays to lepton pairs are very likely to be measured.

TABLE V: The helicity dependent decay widths and branching fractions with Cut I.

	$\Gamma_{e^+e^-\gamma}(10^{-7}\text{GeV})/Br(10^{-4})$	$\Gamma_{\mu^+\mu^-\gamma}(10^{-7}\text{GeV})/Br(10^{-4})$	$\Gamma_{\tau^+\tau^-\gamma}(10^{-6}\text{GeV})/Br(10^{-3})$
flip	4.29/1.04	4.30/1.04	0.3/0.07
non-flip	0.00/0.00	1.37/0.34	13.1/3.19

From Fig. 4 we notice that the contributions from muon and electron helicity non-flip processes are negligible in Higgs radiative decays. This is not a surprise, since in fact the helicity flip events are mainly induced by the loop diagrams. For tree diagrams, however, the largest contribution comes from the soft photon radiation where muon pairs are produced back-to-back and photon is collinear to one of them, which leads to non-flip helicities of the muon pairs. The detailed helicity dependent results for decay width and branching ratio are given in Table V.

The backgrounds of Drell-Yan+ISR and Drell-Yan+FSR are shown in Table IV. Among Drell-Yan + ISR processes, $pp \rightarrow Z\gamma \rightarrow \ell\bar{\ell}\gamma$ has a peak around the Z boson

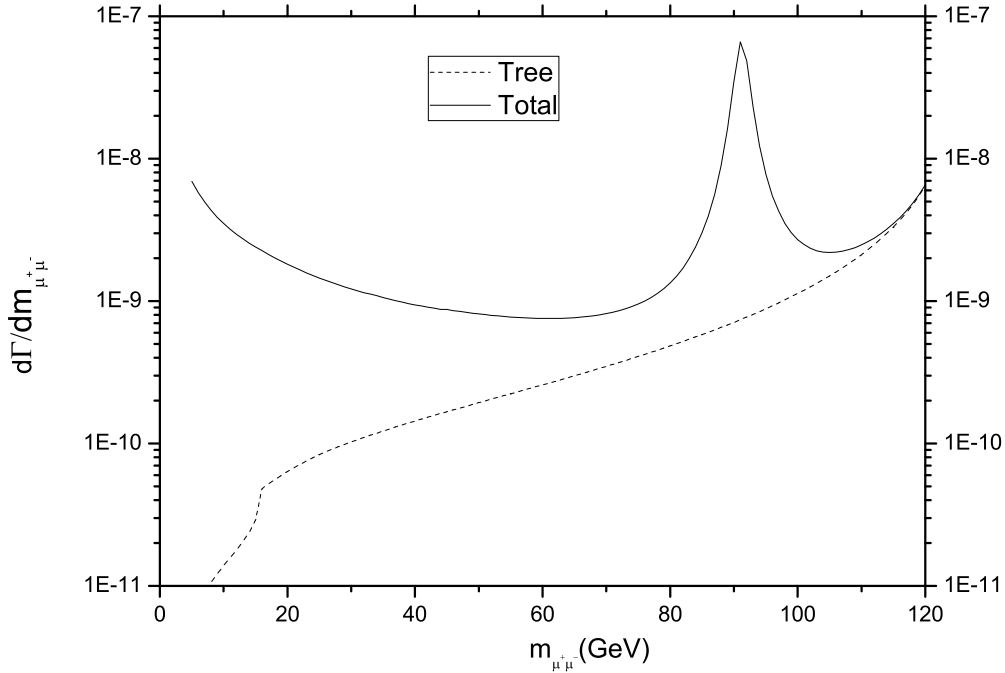


FIG. 3: The $\mu\bar{\mu}$ invariant mass distributions of Higgs decay to $\mu\bar{\mu}\gamma$. Here, the premise of Cut I is taken and the Higgs mass is set to be 125.5 GeV.

mass shell. While for Drell-Yan + FSR processes, the value of $m_{\ell\bar{\ell}\gamma}$ in scope of 115-180 GeV ensures the intermediate particle to be virtual. Hence, for our concerned issue the ISR background is bigger than that of FSR. From Table IV we notice that these two main backgrounds are in order of 10^{-1} pb with actual experimental cuts for signal production. Furthermore, to enhance the signal tagging efficiency and suppress the background, one can perform the measurement on muon pair with flip helicities and invariant mass in scope of 75 GeV to 100 GeV, where half of the Cut I events with photon energy lying in 20 GeV to 40 GeV will be produced because of the Z-pole effect as shown in Fig. 4. Apart from the Drell-Yan background, there are still other processes, like $gg \rightarrow \ell\bar{\ell}\gamma$, contribute to the background. However, they are not evaluated in this work, due to not only detailed background analyses need more works, but superficially these processes

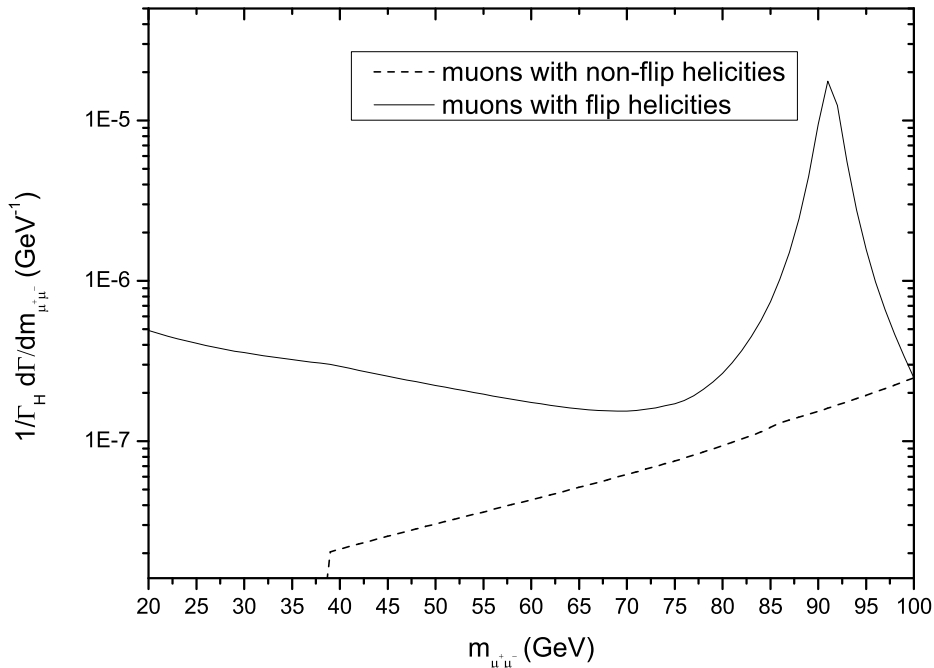


FIG. 4: The $\mu\bar{\mu}$ invariant mass distributions of the Higgs radiative decay to muon pair with different helicities, the flipped ($-+$ and $+-$) and non-flipped ($--$ and $++$) cases. Here, the premise of physical condition Cut II is adopted.

are higher order ones.

IV. CONCLUSIONS

In this paper, the Higgs radiative decays to lepton pairs processes $H \rightarrow \ell\bar{\ell}\gamma$ ($\ell = e, \mu, \tau$) are investigated up to next-to-leading order in perturbative expansion in electroweak interaction. The branching ratios and decay widths are calculated in polarization summed and separated cases with certain physical constraints. The physical Cuts are imposed in the calculation in order to mimic the experimental conditions and pro-

mote the significance of the signal. Numerical result shows that the branching ratios of $H \rightarrow \ell\bar{\ell}\gamma$ ($\ell = e, \mu$) processes are at order of 10^{-4} , some two times larger than that of $H \rightarrow \gamma Z \rightarrow \gamma\ell^+\ell^-$ ($\ell = \mu$ or e) process, while the branching fraction of $H \rightarrow \tau\bar{\tau}\gamma$ process is an order of magnitude higher. Our calculation indicates that although the Z-pole effect is overwhelming, the photon conversion to lepton pairs process is not negligible, especially when the lepton pair with a minimum opening angle. Since the Higgs radiative decays to electron and muon pairs have branching ratios of order 10^{-4} , by virtue of the helicity measurement and Z-pole constraint, it is expected that the signals of these processes will be observed in accumulated data or in the next run of the LHC experiment, provided the Standard Model Higgs is indeed about 125 GeV.

Recently, the CMS Collaboration made a progress in measuring $H \rightarrow \tau\bar{\tau}$ process [26]. Due to the large coupling of tau to Higgs boson, unlike the electron or muon pair radiative production, the tau pair radiative production in Higgs decay is mainly induced by the leading order process in electroweak interaction. However, the helicity measurement and Z-pole constraint may also be helpful to measure the Higgs radiative decay to tau pairs in NLO process.

Finally, we have also checked the W decoupling assumption in this work by taking the zero mass limit of the W boson, and find that the W-loop contribution does not decouple from the processes of Higgs radiative decays to lepton pairs in the dimensional regularization scheme.

Note added: while this paper was submitted, Dicus and Repko post a preprint on the reanalysis of Higgs radiative decay to electron-positron pair [27].

Acknowledgements: This work was supported in part by the National Natural Science Foundation of China(NSFC) under the grants 10935012, 10821063 and 11175249.

-
- [1] G. Aad, *et al.*, the ATLAS Collaboration, Phys.Lett. **B 716**, 1(2012).
- [2] S. Chatrchyan, *et al.*, the CMS Collaboration, Phys.Lett. **B716**, 30(2012).
- [3] A. Aabbasabadi, D. B. Chao, D. A. Dicus, and W. W. Repko, Phys. Rev. **D55**, 5647(1997).
- [4] A. Aabbasabadi, Wayne. W. Repko, Phys. Rev. **D62**, 054025 (2000).
- [5] Ana Firan and Ryszard Stroynowski, Phys. Rev. **D76**, 057301 (2007).
- [6] Chong-Sheng Li, Shou-Hua Zhu, and Cong-Feng Qiao, Phys. Rev. **D57**, 6928 (1998).
- [7] R. Gastmans, S. L. Wu, T. T. Wu, [arXiv:hep-ph/1108.5322].
- [8] R. Gastmans, S. L. Wu, T. T. Wu, [arXiv:hep-ph/1108.5872].
- [9] G. Passarino and M. J. G. Veltman, Nucl. Phys. **B160**, 151 (1979).
- [10] William J. Marciano, Cen Zhang, Scott Willenbrock, Phys. Rev. **D85**, 013002 (2012)
- [11] Hua-Sheng Shao, Yu-Jie Zhang, Kuang-Ta Chao, JHEP 01, 053(2012)
- [12] Da Huang, Yong Tang, Yue-Liang Wu, Commun. Theor. Phys. 57, 427(2012)
- [13] M. Shifman, A. Vainshtein, M.B. Voloshin, V. Zakharov. Phys. Rev. **D85**, 013015 (2012)
- [14] Athanasios Dedes, Kristaq Suxho, [arXiv:hep-ph/1210.0141].
- [15] T. Hahn, Comput. Phys. Commun. **140**, 418 (2001).
- [16] R. Mertig, M. Bohm and A. Denner, Comp. Phys. Comm. **64**, 345 (1991).
- [17] T. Hahn and M. Pérez-Victoria, Comput. Phys. Commun. **118**, 153 (1999).
- [18] A. Denner, Fortschr. Phys. **41**, 307(1993).
- [19] R. Kleiss and W. J. Stirling, Nucl. Phys. **B262**, 245(1985); Zhan Xu, Da-Hua Zhang and Lee Chang, Nucl.Phys. **B291**, 392 (1987).
- [20] Cong-Feng Qiao, Phys. Rev. **D67**, 097503 (2003); C.-H. Chang, J.-X. Wang and X.-G. Wu, Phys.Rev. **D77**, 014022 (2008).
- [21] K. Nakamura, *et al.*, Particle Data Group, J. Phys. **G37**, 075021 (2010).
- [22] S. Dittmaier, *et al.*, arXiv:1101.0593 [hep-ph].
- [23] The CMS Collaboration, CMS-PAS-HIG-12-049.
- [24] J. S.Gainer, W.-Y. Keung, I. Low, and P. Schwaller, Phys. Rev. **D86**, 033010(2012).

- [25] A. Pukhov, CalcHEP 2.3: MSSM, structure functions, event generation, batchs, and generation of matrix elements for other packages (2004). [arXiv:hep-ph/0412191].
- [26] Roger Wolf, Search for the SM Higgs Boson in Di- τ Final States at CMS, Hadron Collider Physics Symposium, Kyoto, 2012.
- [27] Duane A. Dicus and Wayne W. Repko, Phys.Rev. **D87**, 077301(2013).